Photochemical Processes Induced by Vibrational Overtone Excitations: Dynamics Simulations for *cis*-HONO, *trans*-HONO, HNO_3, and HNO_3-H_2O†

Y. Miller,‡ G. M. Chaban,§ B. J. Finlayson-Pitts,|| and R. B. Gerber*,‡,||

Department of Physical Chemistry and Fritz Haber Research Center, The Hebrew University, Jerusalem 91904, Israel, NASA Ames Research Center, Moffett Field, CA 94035, and Department of Chemistry, University of California, Irvine, CA 92697

Received: October 19, 2005; In Final Form: November 25, 2005

Photochemical processes in HNO_3, HNO_3-H_2O, and *cis*- and *trans*-HONO following overtone excitation of the OH stretching mode are studied by classical trajectory simulations. Initial conditions for the trajectories are sampled according to the initially prepared vibrational wave function. Semiempirical potential energy surfaces are used in "on-the-fly" simulations. Several tests indicate at least semiquantitative validity of the potential surfaces employed. A number of interesting new processes and intermediate species are found. The main results include the following: (1) In excitation of HNO_3 to the fifth and sixth OH-stretch overtone, hopping of the H atom between the oxygen atoms is found to take place in nearly all trajectories, and can persist for many picoseconds. H-atom hopping events have a higher yield and a faster time scale than the photodissociation of HNO_3 into OH and NO_2. (2) A fraction of the trajectories for HNO_3 show isomerization into HOONO, which in a few cases dissociates into HOO and NO. (3) For high overtone excitation of HONO, isomerization into the weakly bound species HOON is seen in all trajectories, in part of the events as an intermediate step on the way to dissociation into OH + NO. This process has not been reported previously. Well-established processes for HONO, including cis−trans isomerization and H hopping are also observed. (4) Only low overtone levels of HNO_3-H_2O have sufficiently long liftimes to be spectrocopically relevant. Excitation of these OH stretching overtones is found to result in the dissociation of the cluster H hopping, or dissociation of HNO_3 does not take place. The results demonstrate the richness of processes induced by overtone excitation of HNO_x species, with evidence for new phenomena. Possible relevance of the results to atmospheric processes is discussed.

I. Introduction

Interest in the dynamics of gaseous nitric acid (HNO_3), nitrous acid (HONO), and the nitric acid−water complex (HNO_3-H_2O) is in part due to their role in the chemistry of the upper and lower atmosphere. These molecules are present in the earth's atmosphere and are involved in chemical reactions which influence urban air pollution[1] and stratospheric ozone depletion.[2,3] It is therefore important to understand the mechanisms of the photolysis of these molecules. Nitric acid and nitrous acid have strong hydrogen bonding interactions and, in the presence of water, form complexes. This background has motivated intensive studies of the photolysis of the molecules and their complexes.

Three different mechanisms of photodissociation of HNO_x molecules into HO + NO_x have been reported. The first mechanism involves electronic transition, the second involves excitation to electronic states via initial vibration excitation in the ground-state potential, and the third mechanism involves visible excitation of the OH stretching vibration overtone transitions.

Electronic excitation of HNO_x and HNO_x-H_2O has been studied in numerous laboratory experiments[4−13] of photodissociation of HNO_3 and water-clustered HNO_3 in the ultraviolet (UV) region, and UV photodissociation of HONO has also been studied[14−17] experimentally as well. Photochemistry in the UV region of HONO and of HNO_3 has been examined theoretically. For example, vertical excitations to different electronic excited states of HNO_3 have been computed by ab initio calculations.[18−20] Staikova and Donaldson[20] used ab initio and density functional theory (DFT) calculations to estimate vertical excitations to different electronic excited states of HNO_x ($x = 2, 3, 4$) and their hydrates. Electronic photodissociation from specific vibrational levels of the excited electronic states has been studied both experimentally[21−25] and theoretically.[26−28] However, the processes induced by electronic excitations are still not well-understood quantitatively, and electronic potential energy surfaces of the systems studied here are not available yet. As a result, dynamics simulations of these systems have not been performed.

A second mechanism for dissociation of HNO_3 and HONO is vibrationally mediated photodissociation. In this case, the fragmentation of the excited molecules proceeds via vibrational excitation in the ground electronic state followed by excitation to an electronically excited state, i.e., this process requires two photons. For example, the vibrationally induced photochemistry of *trans*-HONO was studied experimentally[29−31] using the OH stretching overtone transitions on the ground-state potential. This mechanism has also been studied experimentally[32−35] for HNO_3. This mechanism for overtone-enhanced photodissociation, which

† Part of the special issue "John C. Light Festschrift".

* Corresponding author. Tel.: 972-2-6585732. Fax: 972-2-6513742. E-mail: benny@fh.huji.ac.il.

‡ The Hebrew University.

§ NASA Ames Research Center.

|| University of California.

10.1021/jp0559940 CCC: $33.50
Published on Web 01/05/2006

involves absorption of two photons, is unlikely to be important in the atmosphere because of the relatively low light intensities. However, Donaldson et al.[36] proposed that it could generate HO_x under some conditions in polar regions where there is high attenuation of UV radiation.

A third mechanism for dissociation of OH-containing atmospheric species such as HONO and HNO_3 was suggested by Donaldson et al.[37,38] This mechanism involves visible excitation of high OH stretching vibration overtone transitions of the atmospheric molecules, followed by dissociation. An overtone of the OH stretching vibration is excited, and the dissociation of the N−O bond occurs because of the energy flow out of the OH stretching mode into the HO−NO_2 coordinate. Although overtone transitions are intrinsically weaker than the fundamentals, their higher energy places them in the visible region of the solar spectrum where the sunlight intensity is larger.[1] Theoretical studies of the photodissociation of HNO_3 involving state-selective excitation of the OH single-bond stretch were carried out by using a two-dimensional model of HNO_3 in the ground-state potential[39] and the three-dimensional model of HNO_3 in the ground-state potential.[40−42] In a recent combined theoretical and experimental study,[43] the vibrational predissociation of the weakly bound HOONO was observed by following the first OH overtone excitation. Theoretical studies of photodissociation of HONO involving the OH stretching overtone excitation in the ground state were carried out by the group of Thompson.[44−46] They[44−47] used empirical potentials for classical trajectory calculations in order to study the dissociation of HONO, the cis−trans isomerization of HONO, and the intramolecular vibrational energy redistribution (IVR) in HONO. These theoretical studies support the mechanism of the photodissociation of the N−O bond in HONO following overtone excitation of the OH stretching mode.

However, these potentials have not been used to date for dynamic simulations of larger systems such as HNO_3 and HNO_3−$(H_2O)_n$, $n = 1-3$. An analytical potential energy surface was developed[48] for HNO_3 in order to study the IVR using molecular dynamics simulations. This potential is fitted to describe dissociation of the molecule but cannot describe other reaction channels for HNO_3. Another example is the overtone-induced dissociation of HNO_4 which was studied by Staikova et al.[49] by using DFT calculations at the B3LYP/6−3611++G (3df, 3pd) level of theory. However, this study[49] does not present molecular dynamics simulations. Furthermore, while the potentials used describe dissociation of HNO_4, they do not address other reaction channels such as isomerization.

The current study presents classical trajectory simulations of HNO_3, HNO_3−H_2O, and *cis*- and *trans*-HONO, by using the semiempirical PM3 potential energy surface (PES) to study the direct OH stretching overtone-induced behavior of these atmospherically relevant molecules. The overtone transitions of the OH stretching vibration were calculated by using the anharmonic CC−VSCF method.[50,51] The advantage of the PM3 potential for the purpose of this study is that this potential is computationally efficient and applicable to relatively large systems. The PM3 potential can also be used to study different reaction channels along the potential energy surface by "on-the-fly" molecular dynamics simulations. As discussed below, the PM3 potentials are at least semiquantitatively valid for most processes and intermediate species involved. Using certain assumptions, we also applied the PM3 potentials to the treatment of homolytic bond breaking. Several new processes and intermediates are predicted using this method, and new insight into the photochemistry of HNO_x and complexes with water are gained.

II. Methodology

A. Potential Energy Surface (PES). Theoretical studies of large systems require not only accurate potentials but also potentials that are not very computationally expensive. For example, Oppel and Paramonov[39−42] used an accurate ab initio potential in order to study the dissociation of the N−O bond in HNO_3, but computed the potential only along 2 degrees of freedom. Ab initio potentials become too costly computationally as the size of the system increases and as the evaluated points cover a higher domain of coordinates. In dynamical simulations, the values of the PES are evaluated thousands of times along the trajectories; therefore by using ab initio potentials, the dynamic simulations become very expensive, especially for large systems. Classical dynamic simulations were carried out by the group of Thompson[44−46] in order to study the cis−trans isomerization and the dissociation of HONO by overtone excitation of the OH stretching vibration. They used several different PES's for the dynamic simulations in three studies.[44−46] In two studies,[44,45] the PES was generated by using the ab initio calculations with a 4-31G basis set[52,53] and by incorporating empirical information where appropriate. In the third study,[46] they used a semiempirical valence bond (EVB) potential for HONO, in which they slightly modified the EVB potential's expression of Chang and Miller.[54] Although these classical molecular dynamics calculations[44−46] are not computationally expensive for a small molecule such as HONO, it is not known for certain whether these potentials are applicable for systems such as HNO_3 and HNO_3−H_2O studied here. It is also not known whether these potentials are too costly to apply to the systems of interest here. Moreover, these fitted potentials cannot sample all the species obtained by the dynamics simulations. An analytic potential was developed by Liu et al.[48] for studying the dissociation of HNO_3 into OH + NO_2; however, this potential cannot probe other reaction channels for HNO_3. In principle, fitted analytical potentials cannot predict new events.

Therefore, one of the objectives of the current study was to use a realistic PES applicable for the systems studied here for the "on-the-fly" simulations and which is capable of describing different channels of reactions also. We applied the PM3 semiempirical electronic structure method[55,56] in order to study the photochemical processes of atmospheric molecules by using classical molecular dynamic simulations. The PM3 potential does not require restriction to eliminate coordinates, and it allows the study of different paths along the PES. PM3 is one of several modified semiempirical neglect of diatomic differential overlap (NDDO) approximation methods.[57] In the PM3 approximation, not all the integrals which are required in the formation of the Fock Matrix are calculated. The three- and four-center integrals are neglected in PM3, whereas one-center and two-center electron integrals are parametrized. Thus, in principle, the PM3 approximation resembles ab initio methods more than the force field methods. The accuracy of PM3 was tested here for HONO and is discussed in section III. As is the case for other single configurational methods, PM3 is not capable of correctly describing the dissociation of molecules into radicals. However, it is useful for examining such processes, since the PM3 description of the elongation of bonds is more correct. If it is assumed that dissociation takes place once the bond has elongated beyond some critical distance, PM3 is then useful in providing insight into this process. Shemesh et al.[58] reported classical molecular dynamics simulations by using the standard PM3 potential for ionic glycine. The results demonstrated fragmentation of glycine into ion radicals. The topic of bond breaking into radicals is detailed in section III for each system.

As for the HNO_3-H_2O complex, the description of hydrogen bonding present in this system is not perfect by the PM3 potential (PM3 is known to give errors for hydrogen bonds),[59−61] but the transition-state structures of its dissociation to HNO_3 and H_2O, obtained by PM3 and MP2/DZP methods, are similar. Therefore, it can be assumed that PM3 possesses the capability to describe the dynamics at least qualitatively.

B. VSCF Calculation of Vibrational Wave Functions. After the harmonic normal-mode analysis was performed by using the standard PM3 for each molecule, the anharmonic wave functions were calculated by using the VSCF and the CC−VSCF methods.[50,51] The potential along each normal mode was computed for a grid of 16 points, and the interactions between each pair of normal modes were obtained on a square grid of 16 × 16 points. The anharmonic effects are considerably important for higher vibrational excited states. Therefore, the overtone transitions of the OH stretching vibrations were computed by using the VSCF and CC−VSCF approximation.[50,51] Miller et al.[62] computed the overtone transitions of the OH stretching vibration of HNO_3, HNO_4, and *cis*- and *trans*-HONO, using the ab initio MP2/TZP energies.[63,64] The computed anharmonic frequencies were found to be in a good agreement with the experimental spectroscopic results for the first, second, and third overtone excitations. The overtone excitations of the OH stretching mode up to $\nu = 4$ have small deviations from the experimental results (see ref 62). As mentioned above, PM3 potentials are more affordable for dynamics simulations than MP2 potentials. For consistency, in this study, we use the PM3 method both for the vibrational state and for the dynamics calculations.

C. Sampling of Initial Conditions. At sufficiently high energy, classical mechanics should provide a reasonable approximation for the dynamics. To apply dynamical mechanism to these processes, it requires sampling of initial conditions for the classical trajectories from the initial wave functions of the excited vibrational states. Several methods were proposed in the literature[65,66] for representing the distribution of classical positions and momenta for a given state. The Wigner distribution function[67] is among the most familiar distribution functions proposed for this purpose. It has several advantages and is extremely useful. However, work done in our group indicates that a more simplistic sampling method can also be adequate, especially for highly excited initial states that are more classical in character.

A first step for sampling the initial coordinates and the initial velocities is calculation of the vibrational states of the OH stretching vibration at the PM3 electronic structure level of theory by using the anharmonic CC−VSCF method.[50,51] Miller et al.[62,68] described this procedure in detail with respect to the vibrational spectroscopy of HONO, HNO_3, HNO_4, HNO_3-H_2O, H_2SO_4, and $H_2SO_4-H_2O$. The wave functions of the normal modes in each vibrational state of the molecule are calculated along the normal coordinate **q**. The weight of each trajectory is given by the following function:

$$W(\mathbf{q}_1, ..., \mathbf{q}_N) = C|\psi_{1\nu}(\mathbf{q}_1) \prod_{j=2}^{N} \psi(\mathbf{q}_j)|^2 \qquad (1)$$

where $(\mathbf{q}_1, ..., \mathbf{q}_N)$ are the normal coordinates of the configuration, $\mathbf{q}_1$ is the normal coordinate of the OH stretching vibration at vibrational state ν, $\mathbf{q}_j$ is the normal coordinate of the individual vibration, N is the total number of the normal modes, and C is a normalization constant. The initial coordinates of the OH stretching vibration were selected from the maxima of the probability of the wave function of the excited vibrational state and from the "tails" of this wave function. The initial normal coordinates of the other vibrations of the molecule were selected from the maxima of the probability of the wave function in the ground vibrational state.

The corresponding momentum values of the normal modes were calculated for each normal mode as follows. For all the normal modes except the excited OH stretching vibration, the momentum was calculated from the zero-point energy of each normal mode. The momentum of the excited OH stretching mode was calculated by the following equation:

$$P = \pm\sqrt{2 \times E_t - 2 \times V(Q_j)} \qquad (2)$$

where E_t is the total energy, namely, the sum of the zero-point energy and the minimum energy of the equilibrium structure, and $V(Q_j)$ is the value of the energy of the wave function in grid point j. For the same structure, the value of momentum of the OH stretching vibration was chosen in the two opposite directions for two different trajectories.

D. "On-the-Fly" Molecular Dynamics (MD) Simulation. In the current study, an "on-the-fly" molecular dynamics method,[69] which is implemented in the electronic structure program package GAMESS,[70−72] was used for the simulations. The procedure of the "on-the-fly" molecular dynamics (MD) method is as follows. At each very small time step of the trajectory, the current potential energy surface, namely, the PM3 potential, is evaluated and the forces are computed. Availability of the analytic derivatives in PM3 is critical in this respect. Then, atoms are moved according to these calculated forces along the potential to a new position on the potential energy surface. This new position is the next time step of the simulation. The forces at this new position are calculated, and the atoms are moved according to these new forces. This procedure continues up to the time at which the simulation is selected to stop. The propagator which is used in the electronic structure program package GAMESS[70] is reported in detail in ref 69. The SCF (RHF) convergence criterion which was used in the simulations is 10^{-9}, whereas the default value which is employed in the standard GAMESS code[70] is 10^{-5}. The convergence criterion of 10^{-9} was tested and found to give accurate force calculations for the time scale of the trajectories for all the current systems which have been studied here. The time step sizes of 0.05 and 0.08 fs were used for the dynamics simulations of HNO_3 and HONO in order to conserve energy during all 100 ps of the simulations, whereas for HNO_3-H_2O, the time step size which was used for all the trajectories was 0.1 fs.

III. Results and Analysis

A. Initial States. The equilibrium geometries of HNO_3, HNO_3-H_2O, and *cis*- and *trans*-HONO were calculated by using the standard PM3 semiempirical electronic structure theory[55,56] in the GAMESS package.[70] The optimized geometries of these molecules are shown in Figure 1. In our recent study,[62] the structures of these molecules were computed using the MP2/TZP ab initio method.[63,64] The calculated structures of these molecules using the PM3 method are similar to those obtained using the ab initio MP2/TZP. The values of the angles and bond distances computed by both methods were very similar, with only small differences. The range of the deviation of the bond lengths of the PM3 method compared with the ab initio MP2/TZP method is ∼0.01−0.1 Å, while the angles deviate by ∼1.1−4.6°.

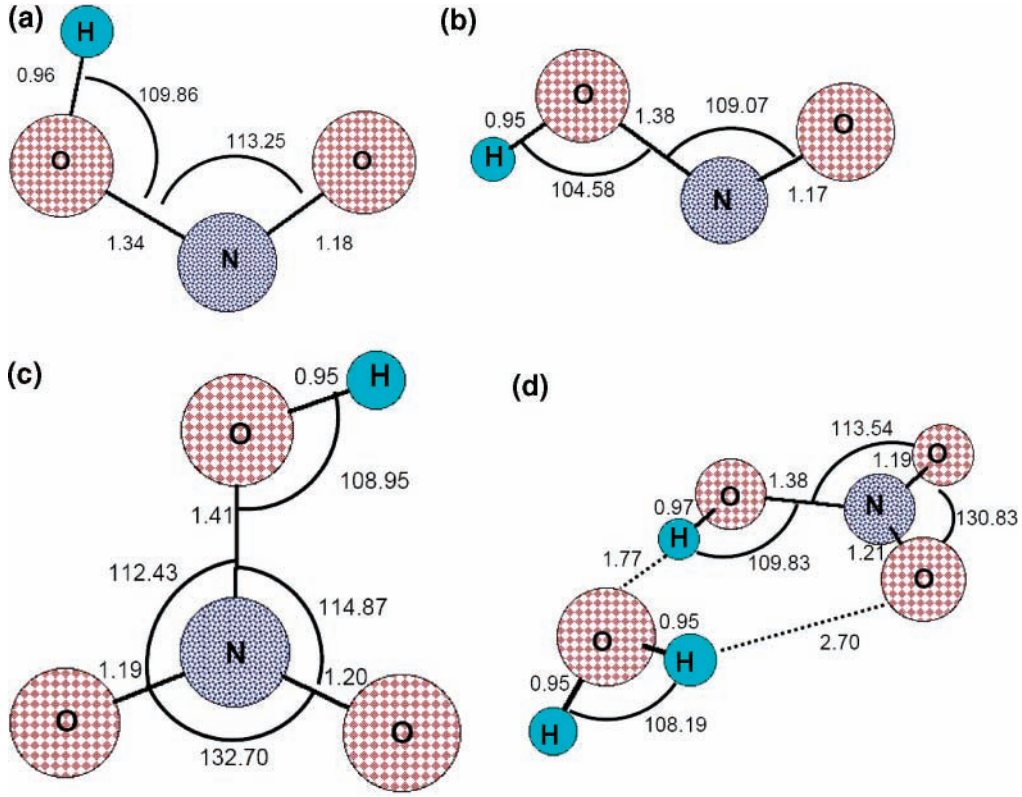

Figure 1. The optimized equilibrium structures of (a) *cis*-HONO, (b) *trans*-HONO, (c) HNO_3, and (d) HNO_3-H_2O. Bond lengths (in angstroms) and angles (in degrees) are given for the PM3 level.

In our recent study, the fundamental frequencies of HNO_3, HNO_3-H_2O, and *cis*- and *trans*-HONO were computed by using the CC−VSCF method[50,51] at the MP2/TZP level.[63,64] Here, we calculated the fundamental frequencies of the current systems using the CC−VSCF approximation with the PM3 electronic structure method. Obviously, the fundamental frequencies which are obtained by using the ab initio MP2/TZP potential are in better agreement with the experiment than the PM3 electronic structure. However, comparison of these two methods did not show large differences for most of the fundamental frequencies of the current systems. The mean deviation of the fundamental frequencies which were calculated by PM3 method for HNO_3 and *cis*- and *trans*-HONO from the MP2/TZP method is 130 cm^{-1}, whereas for HNO_3-H_2O, it is 95 cm^{-1}. In short, structures and frequencies of the current systems calculated by the PM3 method are similar to those calculated at the MP2/TZP level.

The direct OH stretching overtone-induced dynamics of these molecules and the initial conditions for the dynamic simulations were obtained by the procedure described above in section II.C. The overtone transitions used correspond to the vibrational states $\nu = 6$ and $\nu = 7$ for HNO_3, $\nu = 7$ for *cis*- and *trans*-HONO, and $\nu = 3$ for HNO_3-H_2O. It should be noted here that these vibrational states are the highest vibrational levels of the OH stretching vibration that could be obtained by the CC−VSCF calculations. For higher overtone levels, the VSCF calculations fail to converge, indicating that the corresponding states are very short-lived. The OH stretching overtone excitation bands in HNO_3 for the vibrational states $\nu = 6$ and $\nu = 7$ are 20 425.50 cm^{-1} (∼58 kcal/mol) and 24 795.73 cm^{-1} (∼71 kcal/mol), respectively. The OH stretching overtone excitation ($\nu = 7$) bands in *cis*- and *trans*-HONO are 24 351.59 cm^{-1} (∼70 kcal/mol) and 25 338.98 cm^{-1} (∼72 kcal/mol), respectively. Finally, the OH stretching overtone excitation band of $\nu = 3$ is 9593.23 cm^{-1} (∼27 kcal/mol) for the HNO_3-H_2O complex.

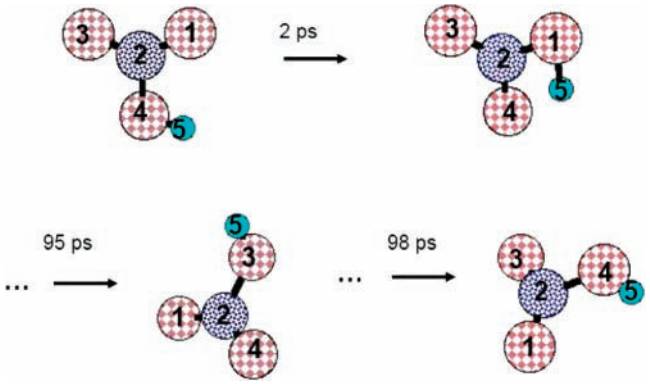

Figure 2. Snapshots of hopping of hydrogen atom in HNO_3. The simulation is evaluated after excitation to the vibrational state $\nu = 7$.

Fourteen trajectories were obtained for HNO_3 in order to study the OH overtone-induced dynamics at $\nu = 6$, and 79 trajectories at $\nu = 7$. For *cis*-HONO, 16 trajectories were obtained at $\nu = 7$, while 80 trajectories for *trans*-HONO were obtained at this vibrational state. Finally, 50 trajectories were computed for HNO_3-H_2O.

B. Intramolecular Hydrogen Hopping in HNO_3. Intramolecular hydrogen hopping was predicted in the present studies for both HNO_3 and HONO. While intramolecular hydrogen hopping in HONO is well-known in the literature, this process has not been previously studied theoretically for HNO_3.

All the trajectories at the vibrational state $\nu = 7$ of HNO_3 exhibited hopping of the hydrogen between the oxygen atoms, whereas only a few trajectories at the vibrational state $\nu = 6$ of HNO_3 exhibited hydrogen transfers. Figure 2 shows typical hydrogen transfers between the three oxygen atoms in HNO_3 at the vibrational state $\nu = 7$ in one simulation. The strength of

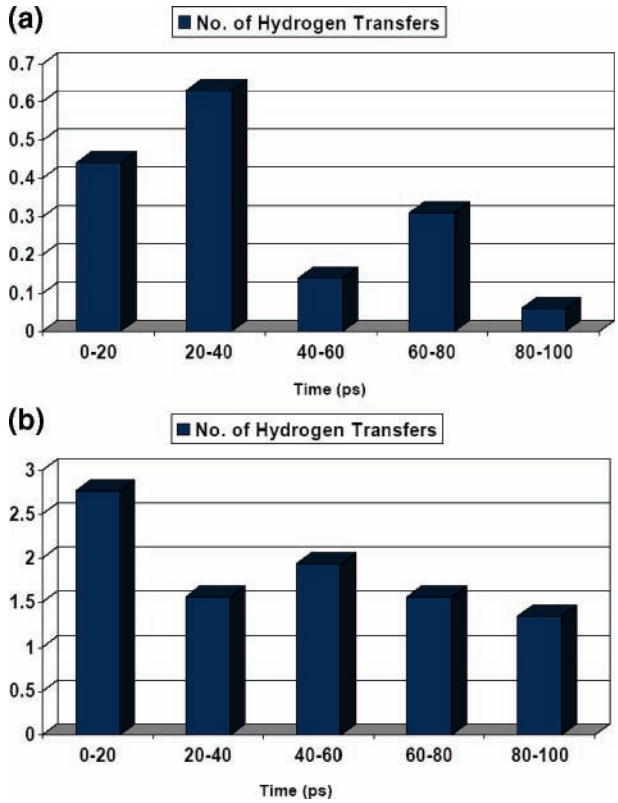

Figure 3. The distribution of the number of the hydrogen hoppings in HNO_3 during the time of the simulation: (a) at the vibrational state $\nu = 6$, (b) at the vibrational state $\nu = 7$.

the H−ONO_2 bond is 423.4 kJ mol^{-1},[73] corresponding to 35 392 cm^{-1}. This is significantly greater than the energy available in the overtones, 20 425.50 cm^{-1} for $\nu = 6$ and 24 795.73 cm^{-1} for $\nu = 7$. Thus, while the hydrogen hops from one oxygen to the next, there must be a significant contribution from energy release due to formation of the new H−O bond as the hydrogen transfers.

Figure 3 describes the distribution of the number of the hydrogen hoppings in HNO_3 in the vibrational states $\nu = 6$ (Figure 3a) and $\nu = 7$ (Figure 3b). The number of the hydrogen transfers at $\nu = 7$ is clearly larger than at $\nu = 6$. The hydrogen is transferred mostly during 20−40 ps of the simulations at $\nu = 6$, while at $\nu = 7$, this process took place mostly during the first 20 ps of the simulations. However, as seen from Figure 3, this phenomenon did not disappear and continued out to at least the 100 ps used in the simulations. Simulations for a longer time (~300 ps) for HNO_3 at the vibrational state $\nu = 7$ show that the hydrogen transfers between the oxygen atoms continues beyond 100 ps. It is possible that for longer times than used in these simulations the intramolecular vibrational energy transfer suppresses this effect.

The predicted migration of the hydrogen between the three O atoms in HNO_3 is supported by an experiment of Donahue et al.[74] who studied the addition of ^{18}OH to $N^{16}O_2$, forming vibrationally excited $HONO_2$. They observed that the ^{18}O atom in the ^{18}OH radical exchanged with ^{16}O, i.e., to form ^{16}OH, suggesting facile H atom transfer in the vibrationally excited $HONO_2$ complex. The hopping of the hydrogen in both HNO_3 and HONO was also studied experimentally by Greenblatt and Howard[75] who reported the rapid oxygen atom exchange between ^{18}OH and $N^{16}O_2$ and $N^{16}O$ reagents using laser magnetic resonance detection of the reagent ^{18}OH and the product ^{16}OH. The experimental results suggested that, during the collisions between the ^{18}OH and $N^{16}O_2$ or $N^{16}O$, the

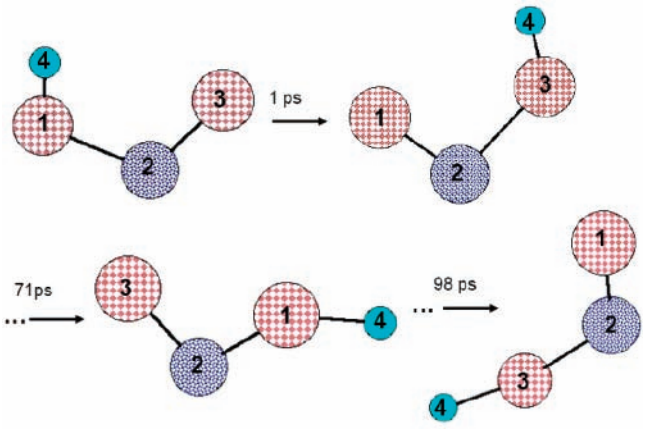

Figure 4. Snapshots of hopping of hydrogen atom in *cis*-HONO. The simulation is evaluated after excitation to the vibrational state $\nu = 7$.

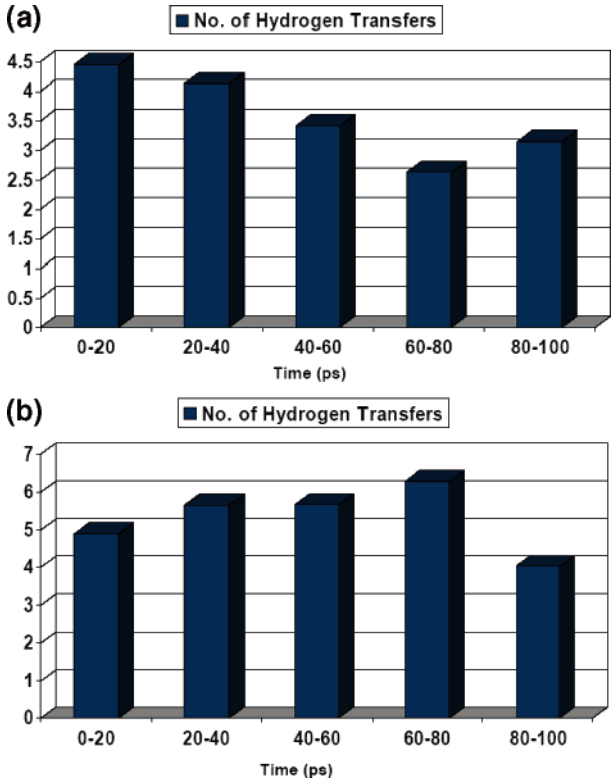

Figure 5. The distribution of the number of the hydrogen hoppings during the time of the simulation at the vibrational state $\nu = 7$: (a) in *cis*-HONO and (b) in *trans*-HONO.

hydrogen atom hops from O atom to O atom. However, our work is the first theoretical study which verifies this phenomenon in the case of overtone-induced excitation.

The hydrogen transfer phenomenon also takes place in *cis*- and *trans*-HONO at $\nu = 7$. Figure 4 presents the snapshots of 1 of 14 trajectories which show the hydrogen hopping in *cis*-HONO at $\nu = 7$. The first hydrogen hop between the O atoms is very fast, occurring at 1 ps; however, the hydrogen also hops at 71 ps and even at 98 ps. Figure 5a describes the distribution of the number of hydrogen transfers in *cis*-HONO at $\nu = 7$ during 100 ps simulations. As seen from Figure 5a, the largest number of hydrogen transfers occurs during the first 20 ps, and then decreases slowly. The phenomenon of the hydrogen transfers is a more frequent event in *cis*-HONO than in HNO_3 (Figure 5a compared to Figure 3b).

Hydrogen hopping in *trans*-HONO at the vibrational state $\nu = 7$ also appears in all 80 trajectories (Figure 5b). Similarly to

the case of *cis*-HONO, the hydrogen hops not only in the first picoseconds, but also at longer time scales within the simulations. Figure 5b shows the distribution of the number of hydrogen transfers in *trans*-HONO at $\nu = 7$ out to 100 ps. There are two significant differences between the *trans*-HONO and both *cis*-HONO and HNO_3 at $\nu = 7$. First, the largest number of hydrogen hops occurs during the first 20 ps for *cis*-HONO and for HNO_3, while for *trans*-HONO, the largest number of hops is at 60−80 ps. Second, the peak number of hydrogen transfers in *trans*-HONO during the time of the simulations is larger than in HNO_3 and in *cis*-HONO (Figure 5b compared to Figure 5a and Figure 3b). These differences can be explained by the differences in the vibrational excitation energy of these species. The overtone excitation of the OH stretching vibration in HNO_3 is 24 795.73 cm^{-1}, and in *cis*-HONO, it is 24 351.59 cm^{-1}, while for *trans*-HONO, the excitation frequency of the overtone of the OH stretching vibration is larger, 25 338.98 cm^{-1}.

Recently, Luckhaus[76,77] used fully coupled six-dimensional (6D) direct quantum dynamics to study the 1,3-intramolecular hydrogen transfer in *cis*-HONO for the first and second OH stretching overtones and reported that the barrier height for this process roughly coincides with the energy of the second OH stretching overtone. We focused studying on $\nu = 7$ for HONO and did not carry out calculations for lower excitation levels. However, our results in combination with those of Luckhaus[76,77] suggest that H hopping is a general phenomenon induced by overtone excitation. Another theoretical study was reported by Herrera and Toro-Labbe,[78] who studied the intrinsic reaction coordinate (IRC)[79,80] using the ab initio and DFT methods. The barrier height of the H atom transfer process was calculated to be 44.12 kcal/mol (15 433.18 cm^{-1}) by Hartree−Fock calculations and 30.75 kcal/mol (10 756.35 cm^{-1}) by DFT calculations. The excitation energy of the $\nu = 7$ vibrational states in *cis*- and *trans*-HONO is above these values and is therefore sufficient to overcome this barrier.

C. Formation of HOONO and HOO + NO from HNO_3. Peroxynitrous acid (HOONO) is an isomer of nitric acid ($HONO_2$), and is an intermediate in the OH + NO_2 reaction. Recently,[81] ab initio MP2/cc-pVTZ level of theory calculations predicted that the HOONO isomer is significantly less stable (by 29.0 kcal/mol) than $HONO_2$. The reaction paths for the formation of the HOONO from OH + NO_2 have been reported extensively in the literature.[81−90] We present here the first classical molecular dynamics simulations of the formation of HOONO from $HONO_2$ via an overtone transition of the OH stretching vibration. In the simulations of 79 trajectories, only 7 trajectories show the formation of the HOONO isomer. Snapshots of 1 of the trajectories can be seen in Figure 6, which shows that the formation of the HOONO isomer involves hopping of the H atom between 2 oxygen atoms. Whether the hopping is a requirement for isomerization of HNO_3 to HOONO to occur is not known. Although hopping was always observed to precede the isomerization in these simulations, it could simply be a separate path that occurs on a shorter time scale than isomerization. The same is true for isomerization of HONO and HNO_2.

In the simulation shown in Figure 6, the HOONO isomer is produced at 15 ps. The mean time scale for the formation of HOONO is 41 ± 8 (1σ) ps (all uncertainties cited in this paper are one standard deviation). The weighted average yield for the formation of HOONO is ∼4%.

It should be noted that, in *all* the simulations of HNO_3 in which the HOONO is produced, the isomer is not converted back into HNO_3, although it is less stable. However, in some of the simulations, HOO and NO radicals were produced from the HOONO isomer (Figure 6). The mechanisms for the HOO + NO reaction have been studied by Zhu and Lin[91] using the DFT/B3LYP method and the transition-state theory calculations. The barrier height which was predicted by Zhu and Lin[91] for the isomerization of HNO_3 to HOONO is 55 kcal/mol (19 239 cm^{-1}), while the OH stretching overtone excitation bands used for $\nu = 6$ and $\nu = 7$ are 20 425.50 cm^{-1} (∼58 kcal/mol) and 24 795.73 cm^{-1} (∼71 kcal/mol), respectively, i.e., above the height barrier. A further interesting process predicted by these simulations is the isomerization between the three different conformers of HOONO: cis−perp, cis−cis, and trans−perp HOONO. Zhao et al.[90] calculated the geometries and the energies of these conformers by using the DFT/B3LYP method. However, these are the first dynamics simulations showing HOONO formation from HNO_3 overtone photochemistry.

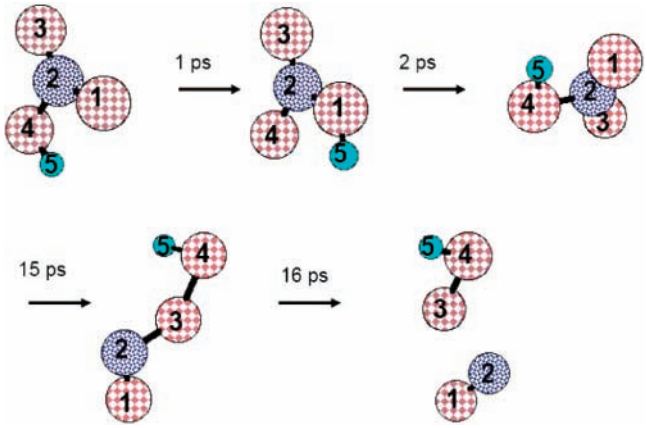

Figure 6. Snapshots of the formation of HOONO and HOO + NO radicals from HNO_3. The simulation is evaluated after excitation to the vibrational state $\nu = 7$.

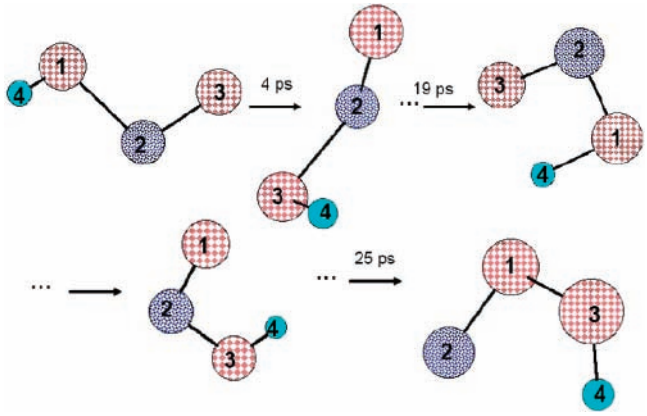

Figure 7. Snapshots of the formation of HOON from *trans*-HONO. The simulation is evaluated after excitation to the vibrational state $\nu = 7$.

D. Formation of HOON (hydroperoxynitrene) from *cis*- and *trans*-HONO. A very interesting result is the formation of the HOON species, which is observed in *all* the dynamics simulations of *cis*- and *trans*-HONO. This isomer appears to be a species somewhere in the range between an unusually strong van der Waals complex and a very weakly chemically bound compound. The snapshots of one of the simulations, which shows the formation of HOON from *trans*-HONO, can be seen in Figure 7. This simulation shows that the process of formation of HOON involves hydrogen transfers. In the simulation in Figure 7, the time at which HOON forms is 25 ps, whereas the mean time scale of the formation of HOON

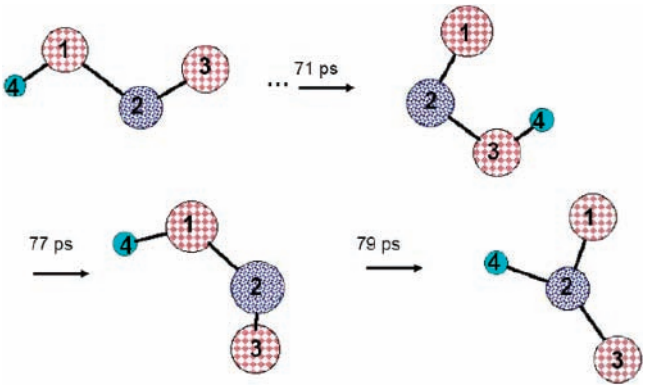

Figure 8. Snapshots of the formation of HNO_2 from *trans*-HONO. The simulation is evaluated after excitation to the vibrational state $v = 7$.

computed for all trajectories is 17 ± 2 ps. Likewise, the simulation of *trans*-HONO, the formation of HOON from *cis*-HONO, also involves hydrogen transfers, and the mean time scale of the HOON formation is 31 ± 7 ps.

It should be noted here that in *all* the simulations of *cis*- and *trans*-HONO, as the HOON is produced it converts very rapidly (in a few femtoseconds) to HONO, and the HOON forms again a few times during the simulations.

To examine if the isomer is an artifact of the PM3 potentials used, the equilibrium structure of this new species was calculated by using the MP2/DZP method. The computed harmonic vibrational frequencies of the *trans*-HOON isomer were as follows: 3734 cm^{-1} (OH stretch), 2459 cm^{-1} (N−O stretch), 728 cm^{-1} (HOO bend), 421 cm^{-1} (O−O stretch), 238 cm^{-1} (NOO bend), and 185 cm^{-1} (out-of-plane vibration). The distances of the N−O, O−O, and O−H bonds are 1.15 Å, 2.02 Å, and 0.98 Å, respectively. The angles NOO and OOH are 118.4° and 95.9°, respectively. It should be noted here that the obtained O−O bond length in the simulations is 1.45 Å. For the *cis*-HOON species, intrinsic reaction coordinates (IRC) calculations using the PM3 potential show a minimum structure where the N−O, O−O, and O−H bonds are 1.12 Å, 1.73 Å, and 0.94 Å, respectively, and the angles NOO and OOH are 115.76° and 108.52°, respectively. Finally, the energy difference between *trans*-HOON and *trans*-HONO as computed by MP2/DZP is 2.0 eV, while the PM3 result is 1.92 eV. This gives some confidence in the PM3 potential surface for this case.

The HOON isomer has not been reported previously in the literature. However, Fueno et al.[92] studied the 1,3-intramolecular hydrogen transfer in the imineperoxide (HNOO) isomer which produces HOON using the MCSCF calculations. The present study demonstrates another pathway to the formation of the HOON isomer upon overtone excitation of HONO.

E. Formation of HNO_2 (hydrogen nitryl) from *cis*- and *trans*-HONO. Snapshots from one of nine simulations of *trans*-HONO showing the formation of HNO_2 isomer can be seen in Figure 8. The formation of the HNO_2 isomer was also observed in four simulations of *cis*-HONO. As in the formation of HOON, the formation of HNO_2 involves hydrogen transfers between the two O atoms in the HONO molecule and then transfer to the N atom to produce the HNO_2 isomer (see Figure 8). The time of formation of the HNO_2 from the *trans*-HONO is 79 ps in the particular simulation shown in Figure 8, while the mean time scale of the formation of this species is about 5 ± 1 ps. The yield of the formation of this species is about 18%.

The mean time scale of the formation of HNO_2 from *cis*-HONO as a precursor is 33 ± 19 ps, and the yield is about 32%. However, the HNO_2 generated in these trajectories usually converts rapidly back to HONO. For example, in only one simulation of *cis*-HONO was HNO_2 produced without back conversion to *cis*-HONO. The same result has been obtained in a few simulations of *trans*-HONO.

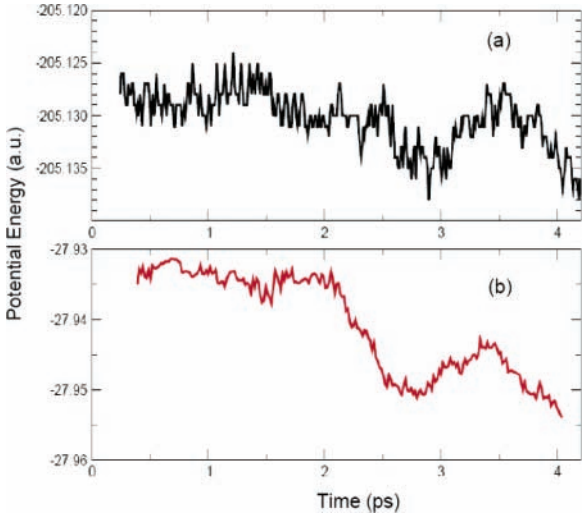

Figure 9. The potential energy during the first 4 ps of the simulation of *trans*-HONO by (a) MP2/DZV level and (b) PM3 method.

The isomerization of HONO to HNO_2 via electronic transitions has been reported previously in the literature. Koch and Sodeau[12] studied the isomerization process of *trans*-HONO to HNO_2 using UV radiation. The authors[12] reported that the isomerization proceeds more readily via *trans*-HONO than *cis*-HONO, because the H atom can move more easily toward the nonbonding electron pair located on the N atom. Nguyen et al.[93] used ab initio calculations and DFT to calculate the overall profile of the potential energy surface (PES) for HNO_2. The authors[93] reported that electronically excited HONO can either undergo 1,2-hydrogen transfer to produce HNO_2 or dissociate into H + NO_2 or HO + NO. They also reported the transition-state structure for the 1,2-hydrogen transfer process and computed the energy barrier for this process as 55.8 kcal/mol (19 518 cm^{-1}). The $v = 6$ and $v = 7$ OH-overtone excitation energies (58.4 and 70.9 kcal/mol) are sufficient to overcome this barrier.

F. Dissociation of the N−O Bond in Atmospheric Molecules. Donaldson et al.[37,38] proposed that atmospheric molecules such as HNO_3 and HONO dissociate as a result of OH stretching overtone excitation in the visible region. In the current work, we tested this general mechanism using realistic (PM3) potentials for HONO, HNO_3, and HNO_3−H_2O systems. As discussed in section II, the PM3 potential is similar to the ab initio potential for these systems but is not expected to correctly describe homolytic bond breaking. To describe dissociation to radicals correctly, one must apply a multiconfigurational technique such as MCSCF. Because of its high cost, we use here a single configuration PM3 potential, but we limit our study to those parts of the PES that are still far from fully dissociated products. Simulations are stopped when the length of the bond which is about to break becomes large (>2 Å), and it can be assumed that dissociation is going to happen. In other words, we do not really look at bond breaking, but rather at a dissociation criterion at sufficient bond elongation.

To test the simulations which were performed using the PM3 potential, we compared the potential energy of *trans*-HONO to calculations which were carried out using the ab initio MP2/DZV method. It is important to note here that the initial structures of the *trans*-HONO by the two methods are very similar. Figures 9 and 10 show the PM3 potential energy of

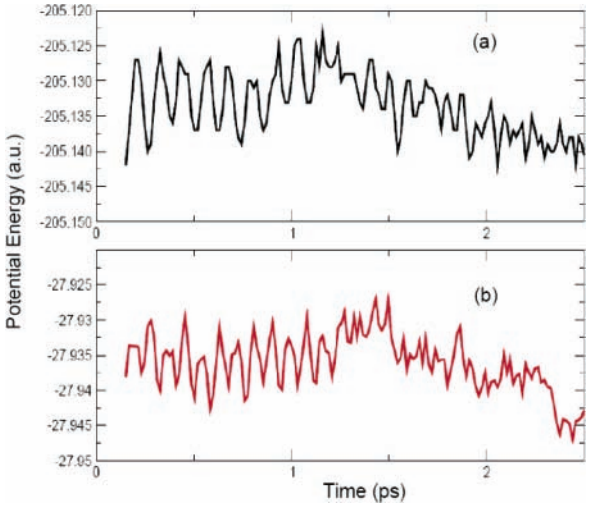

Figure 10. The potential energy during the first 2 ps of the simulation of *trans*-HONO by (a) MP2/DZV level and (b) PM3 method.

trans-HONO versus time (along the trajectory) in comparison with the ab initio MP2/DZV potential for the corresponding trajectory, demonstrating that they are qualitatively similar. For example, as seen from Figure 9, up to 2 ps both MP2 and PM3 potential energies do not change greatly, showing only small fluctuations. At ~2.8 ps, both potentials have a minimum: the value of the PM3 potential energy decreases by ~0.015 au (0.4 eV), while the value of the MP2/DZV potential decreases by ~0.011 au (0.3 eV). At ~3.5 ps, both potentials increase to a maximum point: the value of the PM3 potential energy increases by ~0.007 au (0.2 eV) from the minimum at 2.8 ps, while the value of the MP2/DZV potential increases by ~0.011 au (0.3 eV). In summary, both methods give similar qualitative results for the potential energy surface along the time of the simulation.

It is also interesting to compare the processes that were obtained by these two methods. The first hopping of the H atom in the *trans*-HONO in the MP2/DZV potential occurs at ~4 ps, while this process in the PM3 potential occurs at ~15 ps. Thus, for this process, the time difference is substantial.

During the simulations using both PM3 and MP2 methods, the N−O bond of the *trans*-HONO becomes long enough to indicate dissociation of the N−O bond. The distance for dissociation of the N−O bond was predicted from calculations of the potential energy surface as a function of the N−O bond in *trans*-HONO, using the PM3 method. In these calculations, the distance for dissociation of the N−O bond in *trans*-HONO is 2.602 Å, and the threshold barrier for dissociation is 2.193 eV. The experimental[30] value of the threshold of HONO is 2.0796 eV. Such good agreement is indicative of a reasonably sufficient quality of the PM3 potential in describing breaking of the N−O bond up to its dissociation barrier. It is reasonable to assume that the critical length of the N−O bond at dissociation in *cis*-HONO is almost the same as that in *trans*-HONO. Therefore, we assume that during the simulations the dissociation of the N−O bond in HONO occurs when the N−O bond is elongated up to 2.602 Å.

The dissociation threshold for the N−O bond in HNO_3 was calculated using the PM3 method and the ab initio MP2/DZV level. In the same manner as for the HONO, during the simulations of $HO-NO_2$ we assume that the dissociation of $HO-NO_2$ into $HO + NO_2$ occurs when the N−O bond distance becomes greater than 2.075 Å. As can be seen from Figure 11, the calculated dissociation threshold which was obtained using

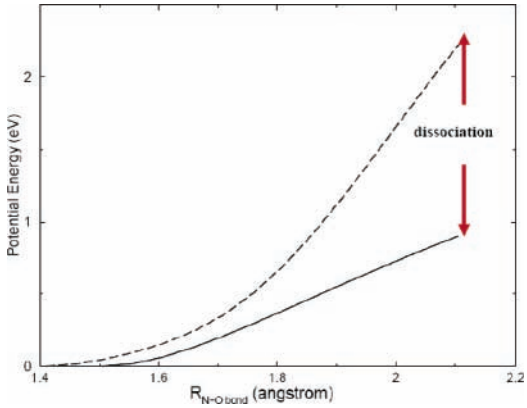

Figure 11. The potential energy as a function of the N−O bond distance in $HO-NO_2$, by MP2/DZV level (solid line) and by PM3 method (dashed line).

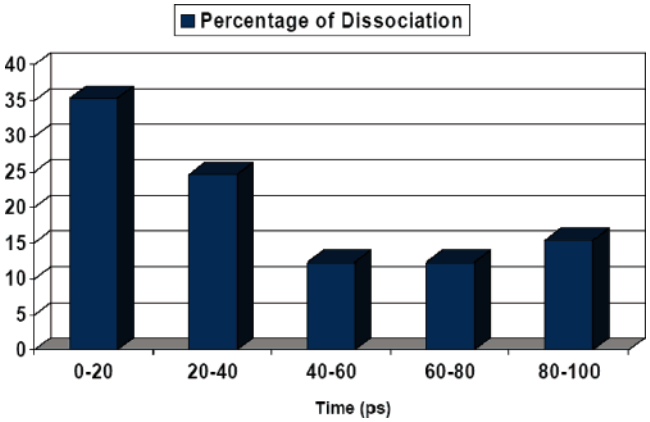

Figure 12. The distribution (in percentage) of the dissociation of the N−O bond in HNO_3 during the time of the simulation. The simulations of 79 trajectories are evaluated after excitation to the vibrational state $\nu = 7$.

the PM3 method (2.08 eV) is higher than the calculated dissociation threshold obtained using the ab initio MP2/DZV method (0.85 eV). In fact, perturbation theories such as MP2 often give barriers and thresholds that are too low. The experimental[94] value is 2.076 eV, again in good agreement with PM3. In addition to the fact that the PM3 threshold value is reasonable, the simulations using this potential with the distance cutoff give systematically reasonable results and support the use of PM3. According to the calculations, the mean time for dissociation of $HONO_2$ at $\nu = 6$ is 31 ± 8 ps, and the probability of this process is ~73%; while the mean time for dissociation at $\nu = 7$ is 36 ± 4 ps, and the probability is ~85%. As expected, the probability of the dissociation of the N−O bond in $HONO_2$ increases with the level of the vibrational state of the OH stretching vibration, i.e., at higher overtone excitations of the OH stretching vibration, the probability that the molecule will dissociate is higher.

It is also interesting to estimate the mean number of hydrogen transfers before the dissociation of the N−O bond occurs. The mean numbers of hydrogen transfers before the dissociation in HNO_3 at $\nu = 6$ and $\nu = 7$ are ~1 and ~4, respectively. Figure 12 shows the distribution of the percentage of the dissociation of the N−O bond in $HONO_2$ during the time of the simulations at $\nu = 7$. For the vibrational state $\nu = 6$, ~29% of the simulations led to dissociation within the first 20 ps, while ~36% led to dissociation in the 40−60 ps time frame. Because the energy flows between the different normal modes during the time of the simulations, including flow of kinetic energy to the H atom, the process of dissociation is delayed. On the other

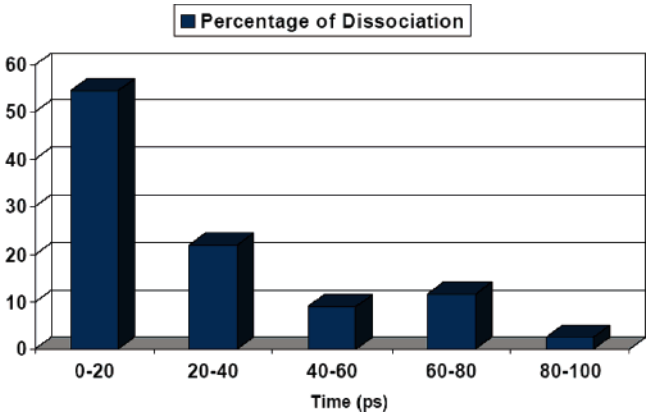

Figure 13. The distribution (in percentage) of the dissociation of the N−O bond in *trans*-HONO during the time of the simulation. The simulations of 80 trajectories are evaluated after excitation to the vibrational state $\nu = 7$.

hand, at the vibrational state $\nu = 7$, for ∼35% of the simulations, the dissociation occurs during the first 20 ps of the simulations. As discussed earlier, the dissociation also continues to occur at longer times.

For *cis*- and *trans*-HONO, the mean times of the dissociations are 31 ± 7 ps and 21 ± 2 ps, respectively. As in the case of HNO_3, hydrogen transfers occur in HONO before the dissociation of the N−O bond. The number of hydrogen transfers before the dissociation of the N−O bond in *cis*-HONO is ∼7, while in *trans*-HONO, it is ∼6. Figure 13 summarizes the time distribution of the N−O bond dissociation yields for *trans*-HONO. Dissociation occurs for ∼38% of the trajectories for *cis*-HONO and ∼55% for trans-HONO. In general, the probability of the dissociation of *cis*- and *trans*-HONO decreases almost exponentially with the time. Koch and Sadeo[12] predicted that the energy flow between the normal modes in *trans*-HONO is faster than in *cis*-HONO, and this prediction explains the higher probability of dissociation of *trans*-HONO compared to *cis*-HONO; this is because excitation energy of $\nu = 7$ in *trans*-HONO is higher than in *cis*-HONO (as mentioned earlier).

G. Cis−Trans Isomerization of HONO. One of the processes extensively described in the literature both experimentally[95−98] and theoretically[44−47,76,77,95,99−105] is the cis−trans isomerization of HONO. We did not focus on this process here, because it has been extensively studied both experimentally and theoretically. However, it is important to note here that our classical molecular dynamics simulations that employed PM3 potentials also predicted the occurrence of cis−trans isomerization, but in the present case, as a result of vibrational OH-overtone excitation.

H. Vibrational Predissociation of HNO_3−H_2O. The 1:1 HNO_3−H_2O cluster has been proposed to be present to a small extent in the troposphere.[106] This cluster may also be a reasonable model for HNO_3 adsorbed on water film or ice surfaces. Therefore, it is of interest to study not only the photodissociation of HNO_3, but also the photodissociation of HNO_3−H_2O. So far, the photodissociation of HNO_3−H_2O following overtone excitation has not been studied experimentally or theoretically. Here, we present the first theoretical study which deals with the mechanism of photodissociation of the complex by the second overtone excitation of the OH stretching vibration of HNO_3 in the complex.

Fifty molecular dynamic simulations were performed for this system using the PM3 semiempirical electronic structure potential[55,56,69] and the direct "on-the-fly" classical dynamics. In *all* the simulations, the complex dissociates in a very short

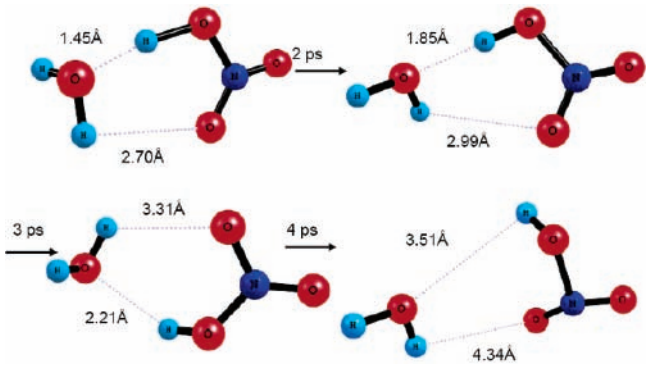

Figure 14. Snapshots of the dissociation of the HNO_3−H_2O. The simulation is evaluated after excitation to the vibrational state $\nu = 3$.

period of the simulation into $HNO_3 + H_2O$. For example, in the specific trajectory of the complex shown in Figure 14, the vibrational predissociation of the complex occurs at 4 ps, while the mean time of the vibrational predissociation is 6 ± 0.5 ps. As discussed earlier, processes such as dissociation and hopping of the hydrogen atom between O atoms are possible for uncomplexed HNO_3 and HONO for sufficiently high overtone excitations ($\nu = 6$ and/or $\nu = 7$). These relevant excited states can be described by the VSCF calculations and could be measured by experiment. In contrast, for $\nu > 3$ in the HNO_3−H_2O complex, VSCF fails to converge, suggesting that the overtone states do not seem to exist or that they have very short lifetimes, making them irrelevant for our purpose. This is due to the strong couplings and the fast intramolecular energy redistribution (IVR) which finally leads to the very fast dissociation of the complex.

Recently, we calculated[62] the anharmonic fundamental frequencies of HNO_3−H_2O using the CC−VSCF approximation[50,51] at the MP2/TZP level.[63,64] The computed frequencies are in good agreement with the spectroscopic experimental results. In the present study, we calculated the anharmonic fundamental frequencies of HNO_3−H_2O, using the standard PM3 potential. The mean percent of the deviation of these frequencies from the frequencies which were obtained by the MP2/TZP method is 3%. These results indicate that the equilibrium structure which is calculated using both potentials is very similar. The energy transfer from the OH stretching vibration in HNO_3 into the H_2O molecule occurs not far from the equilibrium structure; therefore, the anharmonic vibrational frequencies which were obtained by the VSCF calculations using the standard PM3 electronic structure justify the use of the PM3 potential in the current study.

On the other hand, the dissociation of the complex occurs relatively far from the equilibrium structure, and there, PM3 may fail to describe the IVR in the nonequilibrium structure. The computed strength of the HNO_3−H_2O hydrogen bond with respect to the separated fragments using the PM3 method is ∼0.29 eV, whereas using the MP2/TZP method, the value is ∼0.48 eV; the MP2/aug-cc-pVDZ level, which was used by McCurdy et al.[107] predicted ∼0.45 eV, and Tao et al.[106] which used high-level ab initio calculations predicted ∼0.41 eV. These results may indicate that the process of dissociation of the complex using the PM3 method is faster than that using the ab initio potentials, because of the lower energy required by this process. The lifetime of the complex predicted by MP2 calculations which are presumably more accurate should be longer than the lifetime of the complex obtained by using the PM3 method, but qualitatively, we believe that the behavior remains the same.

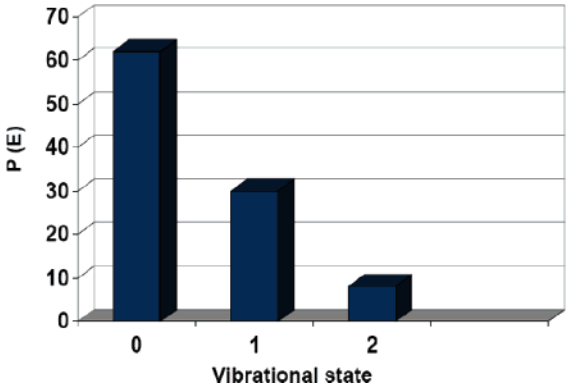

Figure 15. The distribution of the energy left in HNO_3 after the dissociation of HNO_3-H_2O as a function of the vibrational states.

Perhaps the most interesting aspect of the dissociation of the complex HNO_3-H_2O is the vibrational energy remaining in HNO_3 after the separation of the two molecules. Figure 15 shows the probability that the HNO_3 will "fall" to the ground vibrational state after dissociation, using "box quantization" by assigning the energies in the region 1870−2595 cm^{-1} to the vibrational state $\nu = 0$, energies in the region 2595−5056 cm^{-1} to the vibrational state $\nu = 1$, and energies in the region 5056−8122 cm^{-1} to the vibrational state $\nu = 2$. Although the probability that the HNO_3 "falls" to the ground vibrational state $\nu = 0$ is very high (62%), there is 30% probability at $\nu = 1$ (and 8% at $\nu = 2$) of "hot" molecules of HNO_3 being produced in the photodissociation of the complex.

I. Kinetic Energy Flow between Normal Modes in HNO_3. The IVR of HONO has been studied in detail in the literature[44,45] by classical trajectory simulations. To the best of our knowledge, the IVR of HNO_3 has not been reported in the literature. The IVR of HNO_3 is particularly relevant here, to understand the effect of the overtone excitation of the OH stretching vibration in HNO_3 on the energy transfer between normal modes and hence on the dissociation of the N−O bond.

The statistical approach to reaction dynamics is based on the assumption that the IVR takes place in the time scale of a few picoseconds. In terms of temperature, in this time scale the normal modes should equilibrate to a common temperature. The normal modes of the equilibrium structure were used in order to analyze the energy partition into the normal modes during the simulation. It should be noted that the normal mode approximation fails for large displacements from the equilibrium. The mean energy partition into the normal modes was calculated using 77 trajectories with their statistical weights obtained from the distribution function described earlier in section II.C.

The kinetic energy of each mode in each trajectory is calculated during the dynamics and averaged using the distribution function (see section II.C). The temperature of each mode is then obtained from the average kinetic energy in each mode. The temperature of each mode at time t is therefore defined by

$$T(t) = \sum_i \frac{2\omega_i E^i_{\mathrm{kin}}(t)}{k_B} \qquad (2)$$

where the sum is over all the trajectories sampled, ω_i is the statistical weight of the trajectory i, k_B is the Boltzmann factor, and $E^i_{\mathrm{kin}}(t)$ is the kinetic energy of the trajectory i at time t.

Because the fluctuations of the temperature have high frequency, they were smoothed with respect to time variation, and therefore, the temperatures are referred to as effective temperature. Figure 16 shows the effective temperature of different modes as a function of time when the OH stretching vibration is initially excited to $\nu = 7$. These modes were selected from the set of nine modes, since they mostly show an energy transfer behavior. Anticorrelation between effective temperatures (kinetic energy) of two modes shows energy transfer behavior. As seen from Figure 16, the temperature of the excited OH stretching vibration decreases in very few femtoseconds and then remains almost constant. The efficiency of the energy flow between the OH stretching vibration (frequency: 3839.63 cm^{-1}) and the NO_2 asymmetric stretching mode (frequency: 2077.11 cm^{-1}) is due to 2:1 Fermi-resonance between these two modes. The energy of the OH stretching vibration also flows into the ONO_2 out-of-plane vibration. Another efficient energy transfer is obtained between the NO_2 deformation and the NOH bend.

A further approach to probe the energy flow is to examine the couplings between various modes. Miller et al.[68] calculated the values of the anharmonic couplings between modes for H_2SO_4. By using these calculations for HNO_3, the strongest couplings had been obtained between the OH stretching vibration and the NOH torsion mode (the coupling strength is 385 cm^{-1}) and between the OH stretching vibration and the NO_2 symmetric stretching mode (the coupling strength is 1485 cm^{-1}).

Feierabend et al.[108,109] have observed a number of combination bands and overtone combination bands of HNO_3 in the region 2000−8500 cm^{-1}. Their analysis of the frequencies and intensities of the observed transitions indicate that there is some degree of coupling between local modes of HNO_3, persisting at high overtone excitation energies. Feierabend et al.[108,109] measured the following combination modes of HNO_3: the combination mode which includes the OH stretching vibration and the NO_2 asymmetric stretching mode and also the combination of OH stretching vibration with ONO_2 out-of-plane mode. This is experimental evidence for significant coupling between these modes. Feierabend et al.[108,109] also observed that NOH torsion, OH stretching, and NO_2 symmetric stretching modes give the most intense combination bands in the spectra of HNO_3. Combination bands of NO_2 deformation and the NOH bend have not been observed experimentally. However, combination bands of each of these two vibrations individually with the OH stretching vibration were observed experimentally.[108]

The couplings between vibrational modes are essential in IVR and in photoreactions. In our simulations, the energy flows from the OH stretching vibration into different vibrations, and not immediately into the N−O stretching vibration, but eventually, it does at relatively long times. Also, experimental combination modes of the OH stretching vibration and the N−O stretching vibration were not observed by Feierabend et al.[108,109] This may be because there is strong coupling between the other modes in HNO_3, so that the energy does not flow into the N−O stretching vibration immediately and the dissociation of HNO_3 occurs only after considerable delay. Another process which is competitive with the dissociation of HNO_3 appears in our simulation: the hopping of the hydrogen between the oxygen atoms. This process could explain the stagnation of the kinetic energy of the OH stretching vibration (see Figure 16). The barriers to hopping of the H atom are quite small. The H atom receives energy from the excited OH stretching vibration, then "hops" to a different O atom and donates part of the energy to a "new" OH stretching vibration. This process is likely to delay the dissociation of the N−O bond in HNO_3 (and also the isomerization process). As mentioned above, the H mostly "hops" during the first 20 ps, and the mean time scales of the N−O bond dissociation in HNO_3 for $\nu = 6$ and $\nu = 7$ are 31 ± 8 ps and 36 ± 5 ps, respectively. The mean time scale for

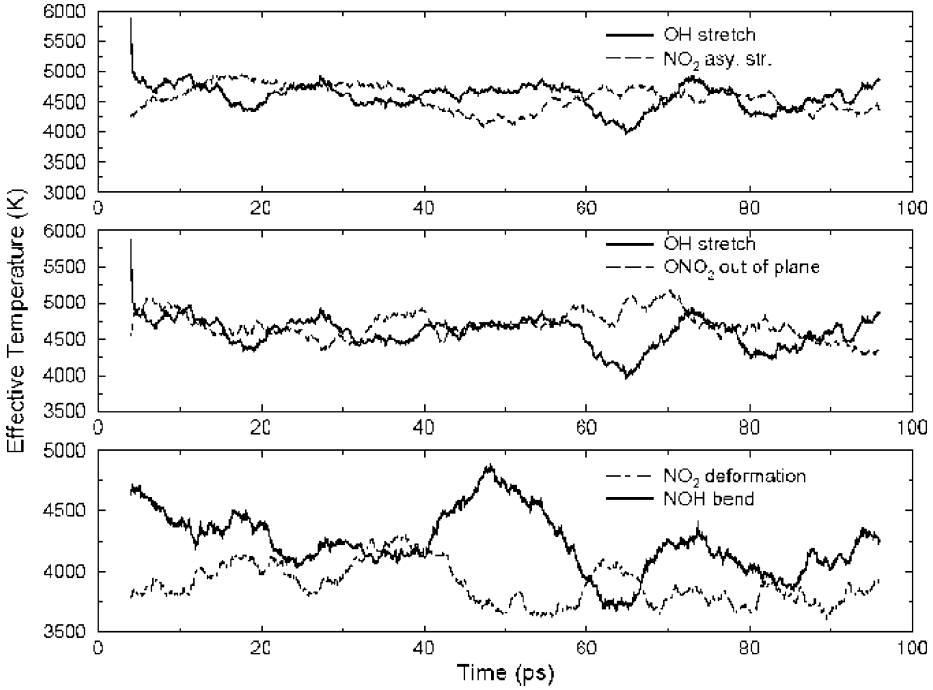

Figure 16. The effective temperature of different normal modes of HNO_3 as a function of time. The OH stretching vibration is initially excited to $\nu = 7$.

the isomerization is 41 ± 8 ps. Therefore, it is possible that IVR is suppresses both processes.

J. Possible Atmospheric Implications. Nitric and nitrous acids play major roles in the chemistry of polluted urban atmospheres.[1] Thus, nitrous acid absorbs light in the region between 300 and 400 nm, wavelengths that reach the earth's surface. This electronic transition leads to dissociation to form the highly reactive OH free radical that drives the chemistry of the atmosphere. Indeed, in polluted urban areas, HONO is the major source of OH not only at dawn but also when averaged over 24 h.[110−112] The present studies show that dissociation can also occur through overtone transitions. However, this is unlikely to be important compared to the electronic photochemistry, which is fast.[1] Perhaps more interesting is the identification of HOON as an intermediate in the overtone photochemistry of HONO, suggesting it may also play a role in the HO + NO recombination in air.

The major oxide of nitrogen directly emitted from combustion sources is NO, which is converted in air to NO_2 and ultimately to HNO_3.[1] Nitric acid is a very "sticky" molecule which undergoes relatively rapid wet and dry deposition either as a gas or in the form of particulate nitrate. As a result, nitric acid is considered the end product of VOC−NO_x oxidations in air. Any processes which result in conversion of HNO_3 back to a photochemically active form of NO_x (e.g., NO, NO_2, HONO) are referred to a "renoxification". The form of nitric acid on surfaces is not well-understood, but likely involves complexes with water. As a result, understanding the photochemistry of nitric acid and its water complexes is important.

The strongest light absorptions for nitric acid electronic transitions are below 290 nm, but there is a weak absorption that extends to large wavelengths, causing dissociation to OH + NO_2. The overtone bands of the ground electronic states are much weaker, but occur at longer wavelengths in the visible region (500−1000 nm) where there is higher solar intensity. However, the overtone photochemistry is unlikely to be sufficient compared to the UV dissociation, except in somewhat unique circumstances. For example, Donaldson, Vaida, Tuck, and co-workers[36−38] suggest that these overtone absorptions can lead to an enhancement in the overall rate of photodissociation in polar regions where the intensity in the UV that leads to dissociation via electronic transitions is reduced. This photochemistry regenerates highly reactive HO_x and NO_x species that can continue to drive atmospheric chemistry.

The present work shows that not only dissociation but also hopping of the hydrogen from one oxygen to another in HNO_3 occurs upon overtone excitation. In the first 100 ps, there are 1−2 hydrogen transfers for HNO_3 excited to $\nu_{OH} = 6$ (Figure 3a). For $\nu_{OH} = 7$, there are about 8−9 hops in the first 100 ps, but the calculations suggest that the hopping continues into longer times (Figure 3b). The fact that the hydrogen is quite mobile suggests the possibility that, during collisions with atmospheric gases, transfer of the hydrogen to the colliding gas molecule might be possible. For example, collision with O_2 could lead to HO_2 + NO_3; the endothermicity of this reaction corresponds to ∼18 660 cm^{-1}, well below the energies of the $\nu_{OH} = 6$, 7 overtones at 20 425 and 24 795 cm^{-1}, respectively. The nitrate (NO_3) radical thus formed photolyzes via two paths, the most important one generating NO_2 + O (^{3}P) (a minor channel in the NO_3 photolysis gives NO + O_2). The oxygen atom adds to O_2 to form O_3, so that the net reaction is

$$(HONO_2)^{\ddagger} + O_2 \rightarrow (HO_2 + NO_3) \xrightarrow{h\nu,\, O_2} HO_2 + NO_2 + O_3$$

In contrast to direct photodissociation to OH + NO_2, this net reaction would also generate an O_3 molecule. Ozone is an important tropospheric constituent in that it is a toxic air pollutant for which air quality standards are set to protect human health as well as agriculture and materials; it is a greenhouse gas; it absorbs UV and is a major source of the OH free radical in air.[1] A similar process could potentially occur in the case of HONO.

Using RRKM calculations, Donaldson et al.[37] estimated that the lifetime of HNO_3 excited to 6 ν_{OH} is ∼150 ps. The calculations presented here are in good agreement with this estimate. Figure 12a, for example, shows that about 75% of

HNO_3 excited to $\nu_{OH} = 6$ dissociates within 100 ps. This can be compared to an average lifetime with respect to collisions at 1 atm pressure with N_2 or O_2 of ~170 ps. At the surface of the earth, then, some of this vibrationally hot HNO_3 may be collisionally deactivated if the quenching efficiency of N_2 and O_2 is large. In this case, the transfer of the "hopping hydrogen" to O_2 may contribute to the overtone photochemistry, although given the magnitudes of the dissociation and collision lifetimes, it would be expected to be a minor pathway. For HNO_3 excited to $\nu_{OH} = 7$, essentially all of the HNO_3 dissociates within 100 ps (Figure 12b) so that collisional deactivation should be less important.

The identification of HOON as an intermediate in HONO photodissociation via the overtone absorption is intriguing in that it suggests it may also be an intermediate in the recombination of OH with NO to form HONO. In an analogous reaction, the OH + NO_2 recombination was only relatively recently recognized to proceed via two channels,[84,113,114] the first corresponding to addition of the OH radical to the nitrogen of NO_2 and the second to addition to an oxygen of NO_2

$$\mathrm{OH} + \mathrm{NO_2} \xrightarrow{\mathrm{M}} \mathrm{HONO_2}$$
$$\rightarrow \mathrm{HOONO}$$

Identification of HOON as an intermediate in the HONO overtone photochemistry suggests that there may also be two paths for the OH + NO reaction, one corresponding to addition of the OH to the nitrogen and the second to addition of OH to the oxygen of NO

$$\mathrm{OH} + \mathrm{NO} \xrightarrow{\mathrm{M}} \mathrm{HONO}$$
$$\rightarrow \mathrm{HOON}$$

Experiments to probe a contribution from this second channel are needed to assess whether it occurs and what the lifetime and fates of the intermediate formed by the OH + NO recombination are under atmospheric conditions. The lifetime of this species is sufficiently short at room temperature that techniques such as matrix isolation spectroscopy might be needed, if indeed this intermediate is observable.

Finally, the photochemistry of nitric acid−water complexes is of interest because of their potential importance on surfaces in the atmosphere. Thus, reactions of oxides of nitrogen such as NO_2 often generate HNO_3 on the surface where it remains adsorbed.[115] There is increasing evidence that some of the adsorbed acid is complexed to water,[116] but the structure, chemistry, and photochemistry of such nitric acid−water complexes remain unknown. However, they are potentially important in the troposphere in that surfaces holding nitric acid are known to generate HONO in the presence of sunlight[117,118] and, under some conditions, react with gaseous NO to generate NO_2.[119−121] The present work suggests that the overtone absorptions will not contribute to renoxification, but rather simply dissociate the HNO_3−H_2O complexes.

Acknowledgment. The authors thank Dr. Eric C. Brown and Prof. Sergey Nizkorodov for helpful and fruitful discussion and Dorit Shemesh for the help in the molecular dynamics simulations. This research was supported by NSF through the Environmental Molecular Science Institute at UC Irvine (grant 0431312), and through CRC project (0209719).

References and Notes

(1) Finlayson-Pitts, B. J.; Pitts, J. N., Jr. *Chemistry of the Upper and Lower Atmosphere−Theory, Experiments, and Applications*; Academic Press: San Diego, 2000.
(2) Solomon, S. *Rev. Geophys.* **1988**, *26*, 131.
(3) Wennberg, P. O.; Cohen, R. C.; Stimpfle, R. M.; Koplow, J. P.; Anderson, J. G.; Salawitch, R. J.; Fahey, D. W.; Woodbridge, E. L.; Keim, E. R.; Gao, R. S.; Webster, C. R.; May, R. D.; Toohey, D. W.; Avallone, L. M.; Proffitt, M. H.; Loewenstein, M.; Podolske, J. R.; Chan, K. R.; Wofsy, S. C. *Science* **1994**, *266*, 398.
(4) Turnipseed, A. A.; Vaghjiani, G. L.; Thompson, J. E.; Ravishankara, A. R. *J. Chem. Phys.* **1992**, *96*, 5887.
(5) Schiffman, A.; Nelson, D. D.; Nesbitt, D. J. *J. Chem. Phys.* **1993**, *98*, 6935.
(6) Myers, T. L.; Forde, N. R.; Hu, B.; Kitchen, D. C.; Butler, L. J. *J. Chem. Phys.* **1997**, *107*, 5361.
(7) Assenmacher, F.; Gutmann, M.; Noack, F.; Stert, V.; Radloff, W. *Appl. Phys. B* **2000**, *71*, 385.
(8) Schlutter, J.; Kleinermanns, K. *Chem. Phys. Lett.* **1992**, *192*, 94.
(9) Jolly, G. S.; Singleton, D. L.; Mckenney, D. J.; Paraskevopoulos, G. *J. Chem. Phys.* **1986**, *84*, 6662.
(10) Cheng, B. M.; Lee, J. W.; Lee, Y. P. *J. Phys. Chem.* **1991**, *95*, 2814.
(11) Lo, W. J.; Lee, Y. P. *J. Chem. Phys.* **1994**, *101*, 5494.
(12) Koch, T. G.; Sodeau, J. R. *J. Phys. Chem.* **1995**, *99*, 10824.
(13) Li, Q.; Huber, J. R. *Chem. Phys. Lett.* **2001**, *345*, 415.
(14) Novicki, S. W.; Vasudev, R. *Chem. Phys. Lett.* **1991**, *176*, 118.
(15) Zhang, J. S.; Amaral, G.; Xu, K. S. *Abstr. Pap. Am. Chem. Soc.* **1999**, *217*, U324.
(16) Shan, J. H.; Wategaonkar, S. J.; Vasudev, R. *Chem. Phys. Lett.* **1989**, *158*, 317.
(17) Wategaonkar, S. J.; Shan, J. H.; Vasudev, R. *Chem. Phys.* **1989**, *139*, 283.
(18) Grana, A. M.; Lee, T. J.; Headgordon, M. *J. Phys. Chem.* **1995**, *99*, 3493.
(19) Bai, Y. Y.; Segal, G. A. *J. Chem. Phys.* **1990**, *92*, 7479.
(20) Staikova, M.; Donaldson, D. J. *Phys. Chem. Chem. Phys.* **2001**, *3*, 1999.
(21) Vasudev, R.; Zare, R. N.; Dixon, R. N. *J. Chem. Phys.* **1984**, *80*, 4863.
(22) Shan, J. H.; Vorsa, V.; Wategaonkar, S. J.; Vasudev, R. *J. Chem. Phys.* **1989**, *90*, 5493.
(23) Dixon, R. N.; Rieley, H. *J. Chem. Phys.* **1989**, *91*, 2308.
(24) Vasudev, R.; Wategaonkar, S. J.; Novicki, S. W.; Shan, J. H. *ACS Symp. Ser.* **1992**, *502*, 279.
(25) Shan, J. H.; Wategaonkar, S. J.; Vasudev, R. *Chem. Phys. Lett.* **1989**, *160*, 614.
(26) Cotting, R.; Huber, J. R. *J. Chem. Phys.* **1996**, *104*, 6208.
(27) Hennig, S.; Untch, A.; Schinke, R.; Nonella, M.; Huber, J. R. *Chem. Phys.* **1989**, *129*, 93.
(28) Oppel, M.; Paramonov, G. K. *Chem. Phys. Lett.* **1999**, *313*, 332.
(29) Holland, S. M.; Stickland, R. J.; Ashfold, M. N. R.; Newnham, D. A.; Mills, I. M. *J. Chem. Soc., Faraday Trans.* **1991**, *87*, 3461.
(30) Reiche, F.; Abel, B.; Beck, R. D.; Rizzo, T. R. *J. Chem. Phys.* **2000**, *112*, 8885.
(31) Reiche, F.; Abel, B.; Beck, R. D.; Rizzo, T. R. *J. Chem. Phys.* **2002**, *116*, 10267.
(32) Fleming, P. R.; Li, M. Y.; Rizzo, T. R. *J. Chem. Phys.* **1991**, *94*, 2425.
(33) Bingemann, D.; Gorman, M. P.; King, A. M.; Crim, F. F. *J. Chem. Phys.* **1997**, *107*, 661.
(34) Sinha, A.; Vanderwal, R. L.; Crim, F. F. *J. Chem. Phys.* **1989**, *91*, 2929.
(35) Sinha, A.; Vanderwal, R. L.; Crim, F. F. *J. Chem. Phys.* **1990**, *92*, 401.
(36) Donaldson, D. J.; Tuck, A. F.; Vaida, V. *Chem. Rev.* **2003**, *103*, 4717.
(37) Donaldson, D. J.; Frost, G. J.; Rosenlof, K. H.; Tuck, A. F.; Vaida, V. *Geophys. Res. Lett.* **1997**, *24*, 2651.
(38) Donaldson, D. J.; Tuck, A. F.; Vaida, V. *Physics and Chemistry of the Earth Part C: Solar−Terrestial & Planetary Science* **2000**, *25*, 223.
(39) Oppel, M.; Paramonov, G. K. *Chem. Phys.* **1998**, *232*, 111.
(40) Oppel, M.; Paramonov, G. K. *Chem. Phys.* **1999**, *250*, 131.
(41) Oppel, M.; Paramonov, G. K. *Appl. Phys. B* **2000**, *71*, 319.
(42) Oppel, M.; Paramonov, G. K. *Chem. Phys. Lett.* **2001**, *339*, 243.
(43) Fry, J. L.; Nizkorodov, S. A.; Okumura, M.; Roehl, C. M.; Francisco, J. S.; Wennberg, P. O. *J. Chem. Phys.* **2004**, *121*, 1432.
(44) Guan, Y. H.; Thompson, D. L. *Chem. Phys.* **1989**, *139*, 147.
(45) Qin, Y.; Thompson, D. L. *J. Chem. Phys.* **1992**, *96*, 1992.
(46) Guo, Y.; Thompson, D. L. *Chem. Phys. Lett.* **2003**, *382*, 654.
(47) Guo, Y.; Thompson, D. L. *J. Chem. Phys.* **2003**, *118*, 1673.
(48) Liu, Y.; Lohr, L. L.; Barker, J. R. *J. Phys. Chem. B* **2005**, *109*, 8304.
(49) Staikova, M.; Donaldson, A. J.; Francisco, J. S. *J. Phys. Chem. A* **2002**, *106*, 3023.
(50) Jung, J. O.; Gerber, R. B. *J. Chem. Phys.* **1996**, *105*, 10332.

(51) Chaban, G. M.; Jung, J. O.; Gerber, R. B. *J. Chem. Phys.* **1999**, *111*, 1823.
(52) Darsey, J. A.; Thompson, D. L. *J. Phys. Chem.* **1987**, *91*, 3168.
(53) Murto, J.; Rasanen, M.; Aspiala, A.; Lotta, T. *THEOCHEM* **1985**, *23*, 213.
(54) Chang, Y. T.; Miller, W. H. *J. Phys. Chem.* **1990**, *94*, 5884.
(55) Stewart, J. J. P. *J. Comput. Chem.* **1989**, *10*, 209.
(56) Stewart, J. J. P. *J. Comput. Chem.* **1989**, *10*, 221.
(57) Jensen, F. *Introduction to Computational Chemistry*; Wiley and Sons: Chichester, 1999.
(58) Shemesh D.; Chaban, G. M.; Gerber, R. B. *J. Phys. Chem. A* **2004**, *108*, 11477.
(59) Harb, W.; Bernal-Uruchurtu, M. I.; Ruiz-Lopez, M. F. *Theor. Chem. Acc.* **2004**, *112*, 204.
(60) Kallies, B.; Mitzner, R. *J. Mol. Model.* **1995**, *1*, 68.
(61) Csonka, G. I.; Angyan, J. G. *THEOCHEM* **1997**, *393*, 31.
(62) Miller, Y.; Chaban, G. M.; Gerber, R. B. *Chem. Phys.* **2005**, *313*, 213.
(63) Pople, J. A.; Binkely, J. S.; Seeger, R. *Int. J. Quantum Chem.* **1976**, *10*, 1.
(64) Dunning, T. H. *J. Chem. Phys.* **1971**, *56*, 716.
(65) Segev, B. *Phys. Rev. A* **2001**, *63*, art. no. 052114.
(66) Garcia-Vela, A. *Chem. Phys.* **2002**, *285*, 245.
(67) Wigner, E. *Phys. Rev.* **1932**, *40*, 749.
(68) Miller, Y.; Chaban, G. M.; Gerber, R. B. *J. Phys. Chem. A* **2005**, *109*, 6565.
(69) Stewart, J. J. P.; Davis, L. P.; Burggraf, L. W. *J. Comput. Chem.* **1987**, *8*, 1117.
(70) http://www.msg.ameslab.gov/GAMESS/GAMESS.html.
(71) Taketsugu, T.; Gordon, M. S. *J. Phys. Chem.* **1995**, *99*, 8462.
(72) Taketsugu, T.; Gordon, M. S. *J. Chem. Phys.* **1995**, *103*, 10042.
(73) Benson, S. W. *Thermochemical Kinetics*, 2nd ed.; John Wiley & Sons: New York, 1976.
(74) Donahue, N. M.; Mohrschladt, R.; Dransfield, T. J.; Anderson, J. G.; Dubey, M. K. *J. Phys. Chem. A* **2001**, *105*, 1515.
(75) Greenblatt, G. D.; Howard, C. J. *J. Phys. Chem.* **1989**, *93*, 1035.
(76) Luckhaus, D. *J. Chem. Phys.* **2003**, *118*, 8797.
(77) Luckhaus, D. *Chem. Phys.* **2004**, *304*, 79.
(78) Herrera, B.; Toro-Labbe, A. *J. Phys. Chem. A* **2004**, *108*, 1830.
(79) Fukui, K. *Acc. Chem. Res.* **1981**, *14*, 363.
(80) Schlegel, H. *Adv. Chem. Phys.* **1987**, *67*, 250.
(81) Dixon, D. A.; Feller, D.; Zhan, C. G.; Francisco, J. S. *J. Phys. Chem. A* **2002**, *106*, 3191.
(82) Burkholder, J. B.; Hammer, P. D.; Howard, C. J. *J. Phys. Chem.* **1987**, *91*, 2136.
(83) Matheu, D. M.; Green, W. H. *Int. J. Chem. Kinet.* **2000**, *32*, 245.
(84) Golden, D. M.; Smith, G. P. *J. Phys. Chem. A* **2000**, *104*, 3991.
(85) Dransfield, T. J.; Donahue, N. M.; Anderson, J. G. *J. Phys. Chem. A* **2001**, *105*, 1507.
(86) Hippler, H.; Nasterlack, S.; Striebel, F. *Phys. Chem. Chem. Phys.* **2002**, *4*, 2959.
(87) Pollack, I. B.; Konen, I. M.; Li, E. X. J.; Lester, M. I. *J. Chem. Phys.* **2003**, *119*, 9981.
(88) Bean, B. D.; Mollner, A. K.; Nizkorodov, S. A.; Nair, G.; Okumura, M.; Sander, S. P.; Peterson, K. A.; Francisco, J. S. *J. Phys. Chem. A* **2003**, *107*, 6974.
(89) Golden, D. M.; Barker, J. R.; Lohr, L. L. *J. Phys. Chem. A* **2003**, *107*, 11057.
(90) Zhao, Y. L.; Houk, K. N.; Olson, L. P. *J. Phys. Chem. A* **2004**, *108*, 5864.
(91) Zhu, R. S.; Lin, M. C. *J. Chem. Phys.* **2003**, *119*, 10667.
(92) Fueno, T.; Yokoyama, K.; Takane, S. *Theor. Chim. Acta* **1992**, *82*, 299.
(93) Nguyen, M. T.; Sumathi, R.; Sengupta, D.; Peeters, J. *Chem. Phys.* **1998**, *230*, 1.
(94) Atkinson, R.; Baulch, D. L.; Cox, R. A.; Hampson, R. F.; Kerr, J. A.; Rossi, M. J.; Troe, J. *J. Phys. Chem. Ref. Data* **1997**, *26*, 521.
(95) Schanz, R.; Botan, V.; Hamm, P. *J. Chem. Phys.* **2005**, *122*, art. no. 044509.
(96) McDonald, P. A.; Shirk, J. S. *J. Chem. Phys.* **1982**, *77*, 2355.
(97) Khriachtchev, L.; Lundell, J.; Isoniemi, E.; Rasanen, M. *J. Chem. Phys.* **2000**, *113*, 4265.
(98) Shirk, A. E.; Shirk, J. S. *Chem. Phys. Lett.* **1983**, *97*, 549.
(99) Richter, F.; Hochlaf, M.; Rosmus, P.; Gatti, F.; Meyer, H. D. *J. Chem. Phys.* **2004**, *120*, 1306.
(100) Richter, F.; Rosmus, P.; Gatti, F.; Meyer, H. D. *J. Chem. Phys.* **2004**, *120*, 6072.
(101) Turner, A. G. *J. Phys. Chem.* **1985**, *89*, 4480.
(102) Coffin, J. M.; Pulay, P. *J. Phys. Chem.* **1991**, *95*, 118.
(103) Bauerfeldt, G. F.; Arbilla, G.; da Silva, E. C. *J. Phys. Chem. A* **2000**, *104*, 10895.
(104) Lee, T. J.; Rendell, A. P. *J. Chem. Phys.* **1991**, *94*, 6229.
(105) Guan, Y.; Lynch, G. C.; Thompson, D. L. *J. Chem. Phys.* **1987**, *87*, 6957.
(106) Tao, F. M.; Higgins, K.; Klemperer, W.; Nelson, D. D. *Geophys. Res. Lett.* **1996**, *23*, 1797.
(107) McCurdy, P. R.; Hess, W. P.; Xantheas, S. S. *J. Phys. Chem. A* **2002**, *106*, 7628.
(108) Feierabend, K. J.; Havey, D. K.; Vaida, V. *Spectrochim. Acta, Part A* **2004**, *60*, 2775.
(109) Feierabend, K. J.; Havey, D. K.; Hintze, P. E.; Vaida, V. in communication.
(110) Winer, A. M.; Biermann, H. W. *Res. Chem. Intermed.* **1994**, *20*, 423.
(111) Alicke, B.; Platt, U.; Stutz, J. *J. Geophys. Res.* **2002**, *107*, art. no. 8196; DOI: 10.1029/2000JD000075.
(112) Stutz, J.; Alicke, B.; Neftel, A. *J. Geophys. Res.* **2002**, *107*, art. no. 8192; DOI: 10.1029/2001JD000390.
(113) Sander, S. P.; Ravishankara, A. R.; Friedl, R. R.; Golden, D. M.; Kolb, C. E.; Kurylo, M. J.; Molina, M. J.; Huie, R. E.; Orkin, V. L.; Moortgat, G. K.; Finlayson-Pitts, B. J. *Chemical Kinetics and Photochemical Data for Use in Atmospheric Studies*; Evaluation Number 14; Jet Propulsion Laboratory, California Institute of Technology, 2003.
(114) Nizkorodov, S. A.; Wennberg, P. O. *J. Phys. Chem. A* **2002**, *106*, 855.
(115) Finlayson-Pitts, B. J.; Wingen, L. M.; Sumner, A. L.; Syomin, D.; Ramazan, K. A. *Phys. Chem. Chem. Phys.* **2003**, *5*, 223.
(116) Dubowski, Y.; Sumner, A. L.; Menke, E. J.; Gaspar, D. J.; Newberg, J. T.; Hoffman, R. C.; Penner, R. M.; Hemminger, J. C.; Finlayson-Pitts, B. J. *Phys. Chem. Chem. Phys.* **2004**, *6*, 3879.
(117) Zhou, X. L.; He, Y.; Huang, G.; Thornberry, T. D.; Carroll, M. A.; Bertman, S. B. *Geophys. Res. Lett.* **2002**, *29*.
(118) Zhou, X. L.; Gao, H. L.; He, Y.; Huang, G.; Bertman, S. B.; Civerolo, K.; Schwab, J. *Geophys. Res. Lett.* **2003**, *30*.
(119) Mochida, M.; Finlayson-Pitts, B. J. *J. Phys. Chem. A* **2000**, *104*, 9705.
(120) Saliba, N. A.; Yang, H.; Finlayson-Pitts, B. J. *J. Phys. Chem. A* **2001**, *105*, 10339.
(121) Rivera-Figueroa, A. M.; Sumner, A. L.; Finlayson-Pitts, B. J. *Environ. Sci. Technol.* **2003**, *37*, 548.